ACS APPLIED MATERIALS & INTERFACES

Research Article

www.acsami.org

Controlled Fabrication of Core–Shell TiO_2/C and TiC/C Nanofibers on Ti Foils and Their Field-Emission Properties

Xuming Zhang,[†] Kaifu Huo,*[,†,‡] Hairong Wang,[‡] Biao Gao,[‡] Jijiang Fu,[‡] Tak-Fu Hung,[†] and Paul K Chu*[,†]

[†]Department of Physics and Materials Science, City University of Hong Kong, Tat Chee Avenue, Kowloon, Hong Kong, China

[‡]School of Materials and Metallurgy, Wuhan University of Science and Technology, Wuhan 430081, China

ABSTRACT: Core–shell TiO_2/C and TiC/C nanofibers are fabricated in situ on Ti and Al ion-implanted Ti substrates by a thermochemical reaction in acetone and the growth mechanism is described. Implantation of Al into Ti leads to in situ growth of TiC/C in lieu of TiO_2/C nanofibers. This is because Al has a higher affinity to oxygen than Ti and Ti reacts preferentially with C to form TiC. The Ti foil serves as both the Ti source and substrate for the core–shell TiO_2/C and TiC/C NFs to ensure strong bonding and small contact resistance between the Ti substrate and the core–shell field emitters. The core–shell TiC/C and TiO_2/C nanofibers have similar morphology and structure, but the TiC/C nanofibers possess better field emission properties with a turn on field (E_{to}) of 2.2 V/μm compared to an E_{to} of 3.2 V/μm measured from the TiO_2/C nanofibers. The enhanced field-emission property of the TiC/C nanofibers is attributed to the high electrical and thermal conductivity of the TiC inner core, which provides a more effective electron transfer pathway between the cathode and C shell emitters.

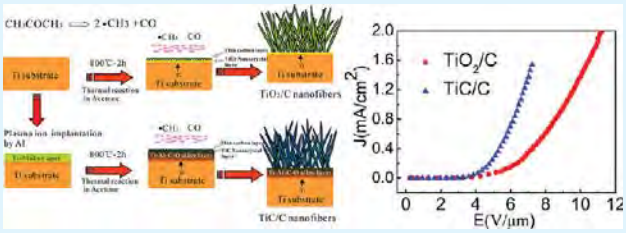

KEYWORDS: *TiO_2/C and TiC/C core–shell nanostructures, fabrication, electron field emission*

INTRODUCTION

Cold field emitters have attracted much attention due to their potential applications to vacuum electronic devices, flat-panel displays, microwave power amplifiers, traveling wave tubes, and X-ray tubes.[1−3] One-dimensional (1D) nanostructures such as carbon nanotubes (CNTs) are considered ideal cold field emitters that can emit electrons under a small applied electric field because of their sharp tips, high aspect ratio, and consequently high field enhancement factor (β).[4−6] In addition to the geometric factors, the intrinsic electrical and thermal conductivity characteristics of the 1D emitters as well as the contact resistance between the nanoemitters and substrate play important roles in the electron emission performance of 1D emitters.[5] A small ohmic contact and strong bonding between the emitters and substrate can ensure easy electron transport from the collector to emitter, thus resulting in a low turn-on field and good field emission (FE) stability. In contrast, poor 1D emitter-substrate contact may cause unreliable field emission and give rise to a very short life span of such a field emission device. Hence, direct growth of 1D emitters such as CNTs on a metal substrate with high electrical and thermal conductivity is a desirable method to achieve good field emission properties.[7] In this case, good bonding between the substrate and the CNTs can reduce the contact resistance to ensure easy electron transportation and at the same time, the heat generated by the emitter and contacting interface can be effectively dissipated by the highly thermal conductive substrate to minimize debonding of emitters from the substrate. Consequently, good field-emission properties are expected from such field emission emitter devices.

Titanium (Ti) is known to have a low contact resistance with CNTs of about an order of magnitude smaller than that of Pd, Pt, Cu, and Au.[8] Thus, Ti is commonly used as a buffer layer during the fabrication of CNTs on metallic or Si substrates.[9] In this paper, we report the controlled fabrication of quasi-aligned core–shell TiO_2/C and TiC/C nanofibers (NFs) on Ti and Al ion-implanted Ti substrates via a simple one-step thermal reaction under acetone vapor at 800 °C. The Ti foil serves as both the Ti source and substrate for the core–shell TiO_2/C and TiC/C NFs to ensure strong bonding and small contact resistance between the Ti substrate and the core–shell field emitters. This configuration bodes well for FE as confirmed by this study. This paper describes a simple method to allow controlled synthesis of core–shell carbon NFs with different inner cores to alter the field emission properties. Although there are many papers reporting the field emission of core–shell 1D nanostructures,[10−12] there are few papers concerned with adjusting the inner core composition and effects of the conductivity of inner core on the field-emission properties of core–shell nanofiber on the same substrate. The introduction of Al by plasma immersion ion implantation (PIII) leads to the in situ growth of TiC/C NFs instead of TiO_2/C NFs on Ti because Al has a higher affinity to oxygen than Ti.[13,14] In

Received: November 28, 2011
Accepted: January 16, 2012
Published: January 16, 2012

comparison with the TiO_2/C NFs, the TiC/C NFs exhibit enhanced field-emission properties with a lower turn-on field, although these two NFs have similar morphology and structure. The enhanced field emission properties can be ascribed to the formation of the highly conductive TiC core and good bonding between the Ti substrate and emitters thereby providing low resistance paths for electron transport from the Ti substrate to the carbon shell emitters. The simple fabrication process and promising FE properties of the core−shell TiC/C NFs render the materials potentially useful in flat panel displays and other vacuum nanoelectronic devices.

EXPERIMENTAL DETAILS

Ti foils (99.6% purchased from Aldrich) were cut to dimensions of 10 × 10 × 1 mm^3 and then polished by SiC paper and ultrasonically cleaned in acetone, ethanol, and distilled water sequentially. The Ti foils were implanted with Al using a plasma immersion ion implanter equipped with a cathodic arc metal ion source at City University of Hong Kong.[15,16] Implantation was conducted at a pulsed high voltage of −20 kV and the cathodic arc conditions were: pulse duration of 300 ms, repetition rate of 10 Hz, arc current of 1 A, and pressure of 2.5 × 10^{-2} Torr. The Ti samples implanted with different amounts of Al (different implantation time) were analyzed by X-ray photoelectron spectroscopy (XPS, Physical Electronics PHI 5802) for elemental depth profiles and chemical states.

The thermochemical reaction between the pristine Ti and Al ion-implanted Ti foil and acetone vapor was conducted on in a horizontal tube furnace. The as-received Ti foils and Al ion-implanted Ti foils were put on a ceramic substrate in the center of an alumina tube. The reactor was purged with argon (Ar) several times to remove residual oxygen and/or moisture before being heated to 800 °C. Acetone was introduced into the chamber with Ar as the carrier gas. The reaction proceeded for 2 h and the sample was cooled to room temperature under flowing Ar. The samples were collected and characterized by glancing angle X-ray diffraction at 1° incidence angle (GAXRD, Philips X' Pert Pro), atomic force microscopy (AFM, Auto-Probe CP, Park Scientific Instruments), field-emission scanning electron microscopy (FE-SEM, JSM-820), transmission electron microscopy (TEM, Philips CM20), and high-resolution TEM (HR-TEM, JEM-2010F). Micro-Raman spectra were acquired using a 514.5 nm argon laser (HR LabRam). The field-emission (FE) properties of the products were measured using a parallel-plate diode configuration in a chamber at a pressure of 1 × 10^{-6} Torr. The NFs fabricated on Ti foil were used directly as the FE cathode and another stainless steel electrode plate was employed as the anode at a sample to anode distance of 200 μm. The high voltage was supplied by a Keithley 248 and the emission currents were measured under different applied voltages by a Keithley 6514 electrometer with an accuracy of 1 × 10^{-11} A.

RESULTS AND DISCUSSION

Images a and b in Figure 1 depict the AFM images of the pristine Ti and Al ion-implanted Ti samples. After Al PIII for 30 min, the surface morphology and surface roughness exhibit no obvious changes. The Al XPS depth profile reveals that Al is distributed in the near surface within a depth of 100 nm (Figure 1c). When the implantation time is increased from 5 to 60 min, the Al concentration in the top 50 nm increases gradually from 7 to 35 at %. The high-resolution Al XPS binding energy (Figure 1d) suggests that Al is mainly in the metallic state with some native oxide on the surface.[17,18]

Figure 2a−d displays the representative FE-SEM images of the products after the thermochemical reaction under gaseous acetone at 800 °C for 2 h. As shown in Figure 2a, quasi-aligned NFs with diameters of about 40−60 nm and lengths up to micrometers are produced on the pristine Ti foil. Similar surface morphology is observed from the NFs synthesized on

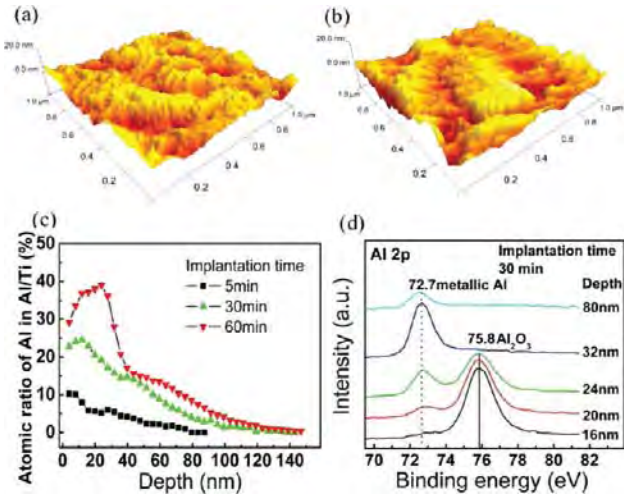

Figure 1. AFM images of the Ti substrate: (a) before and (b) after Al plasma immersion ion implantation (PIII) for 30 min. (c) XPS depth profile of Al after PIII for 5, 30, and 60 min. (d) High-resolution Al 2p spectra acquired at different depths after 30 min Al PIII.

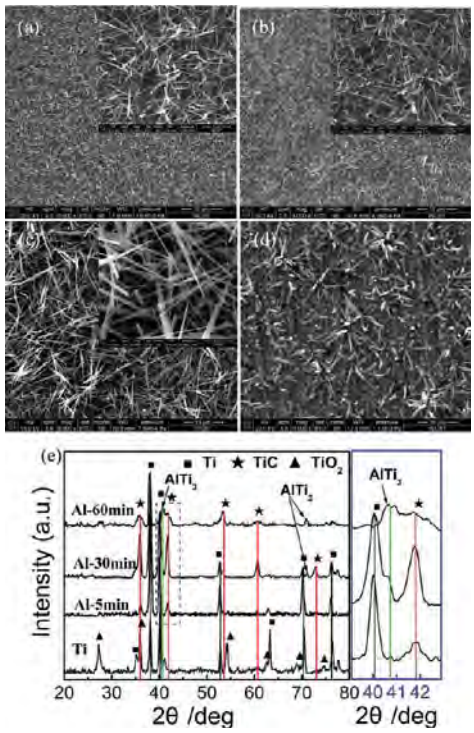

Figure 2. FE-SEM images of the products on (a) pristine Ti and Ti after Al PIII for (b) 5, (c) 30, and (d) 60 min. (e) Corresponding GAXRD patterns of different products shown in a−d.

the Ti foil implanted with Al for 5 min. When the Al ion implantation time is increased to 30 min, longer NFs with larger diameters are formed as shown in Figure 2c. However, when the Al concentration is further increased by extending the Al ion implantation time to 60 min, only sparse and shorter NFs are observed as shown in Figure 2d. Because no particulate catalyst can be observed to adhere to the tip of the NF in all the samples, the thermochemical process appears to have a different mechanism than that of catalyst-assisted vapor−liquid−solid growth.[19] The corresponding GAXRD patterns are

displayed in Figure 2e. With regard to the NFs grown on pristine Ti, the main diffraction peaks can be indexed to tetragonal rutile TiO_2 (JCPDS card: No 21−1276) in addition to those from the Ti substrate.[20] However, for the NFs grown on the Al ion-implanted Ti foil, the characteristic peak of rutile TiO_2 located at 27.2° cannot be observed but other peaks at 35.9, 41.7, and 60.4° indexed to cubic TiC (JCPDS card: No 32−1383)[21] appear. In addition, a weak peak at 40.8° attributable to the intermediate phase of $AlTi_3$ (JCPDS card: No 52−0859) can be observed and its intensity goes up with Al implantation time.

Figure 3a−d depicts the Raman scattering spectra and TEM images of the NFs grown on Ti and Al ion-implanted Ti. In the

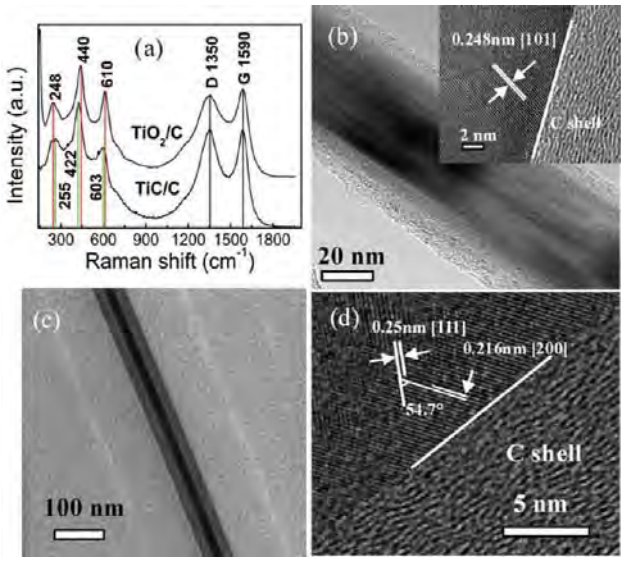

Figure 3. (a) Raman spectra and TEM and HR-TEM images of the core−shell (b) TiO_2/C and (c, d) TiC/C NFs.

range of 150 to 1000 cm^{-1}, the NFs grown on pristine Ti show three characteristic Raman peaks at 248, 440, and 610 cm^{-1} that can be ascribed to the rutile TiO_2 Raman active modes of second-order scattering, E_g and A_{1g} respectively (upper curve in Figure 3a).[20,22] With regard to the NFs grown on Al ion-implanted Ti, the three peaks at 255, 422, and 603 cm^{-1} can be assigned to the vibration signals of TiC (lower curve in Figure 3a).[23] In the range between 1000 and 2000 cm^{-1}, two strong peaks at 1352 and 1588 cm^{-1} corresponding to the D and G bands of amorphous carbon, respectively can be observed for both samples.[24,25] The TEM images of the NF on pristine Ti displayed in Figure 3b clearly indicate the NF is core−shell structure. The core has a uniform diameter of about 20−40 nm and the shell has a thickness of 10−15 nm. The lattice spacing between adjacent lattice planes of the core is approximately 0.25 nm, corresponding to the distance between the two [101] planes of rutile TiO_2. XRD, Raman, and TEM results provide evidence that core−shell TiO_2/C NFs are directly grown on the Ti foil. However, after Al PIII, core−shell TiC/C NFs instead of TiO_2/C NFs are produced. Figures 3c and 3d display typical TEM and lattice-resolution HR-TEM images of the NF shown in Figure 2b, disclosing that the NF grown on Al ion-implanted Ti also exhibits a core−shell structure with a single-crystalline inner core and C shell. The diameter of the core is 25−35 nm and C shell thickness is approximately 15−25 nm. The lattice spacing between adjacent lattice planes of the crystalline core is approximately 0.25 and 0.22 nm, corresponding to the distance between the two [111] and [200] planes of TiC, respectively. The carbon shell in both core−shell TiO_2/C and TiC/C are not crystallized containing nanocrystalline graphite or sp^2 clusters as corroborated by the Raman spectra and HR-TEM images.[25]

In the preparation process, Ti in the TiC or TiO_2 core originates from the Ti substrate and C and O species from the acetone precursors and consequently, the reaction temperature and acetone content in the furnace have an important influence on the morphology of the final products. Figure 4 shows the

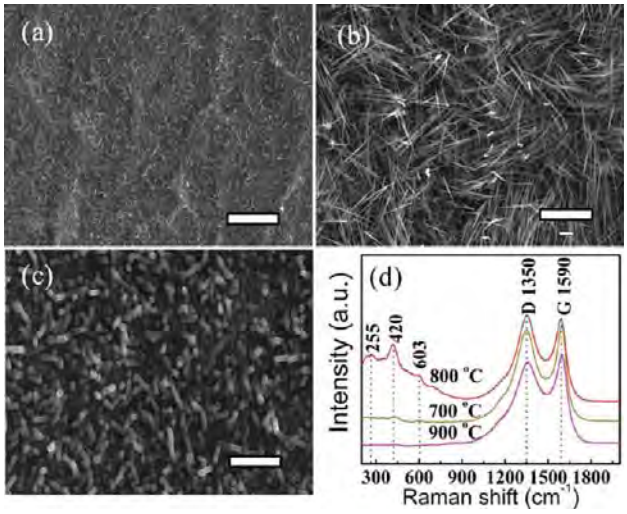

Figure 4. FE-SEM images of the products grown on Ti foils after Al PIII for 30 min at different temperature under flowing acetone (100 sccm): (a) 700, (b) 800, and (c) 900 °C. (d) Corresponding Raman spectra. The scale bar is 10 μm.

morphology evolution of nanofibers with temperature on the Al ion-implanted Ti foil. At a relatively low temperature of 700 °C, short and sparse nanothorns are formed on the substrate as shown in Figure 4a. When the reaction is carried out at 800 °C, dense and longer NFs are in situ grown on the substrate. However, at a higher reaction temperature of 900 °C, only thick and short nanorods can be observed. At 700 °C, the diffusion rate of Ti is relatively small, thereby resulting in the formation of short and sparse nanothorns. On the other hand, at a higher temperature of 900 °C, the decomposition rate of acetone is accelerated and more carbon is deposited on the substrate to form a thick carbon layer. This inhibits diffusion of Ti from the substrate to form TiC NFs and so only thick and short nanorods can be observed at this temperature. This mechanism is corroborated by Raman scattering. The typical carbon Raman vibration modes, D and G bands centered at 1350 and 1590 cm^{-1}, are observed from all three samples. However, the TiC Raman signal is largest from the sample prepared at 800 °C, suggesting that this is the optimized reaction temperature to synthesize the core−shell TiC/C NFs. We have also investigated the influence of the acetone content on the morphology of the final product grown on pristine Ti.[26] With increasing acetone content, the diameter of the core−shell TiO_2/C NF becomes thicker due to the formation of a thicker C shell (results not shown here). The similar phenomenon is observed during the fabrication of core−shell TiC/C NFs on Al ion-implanted Ti.

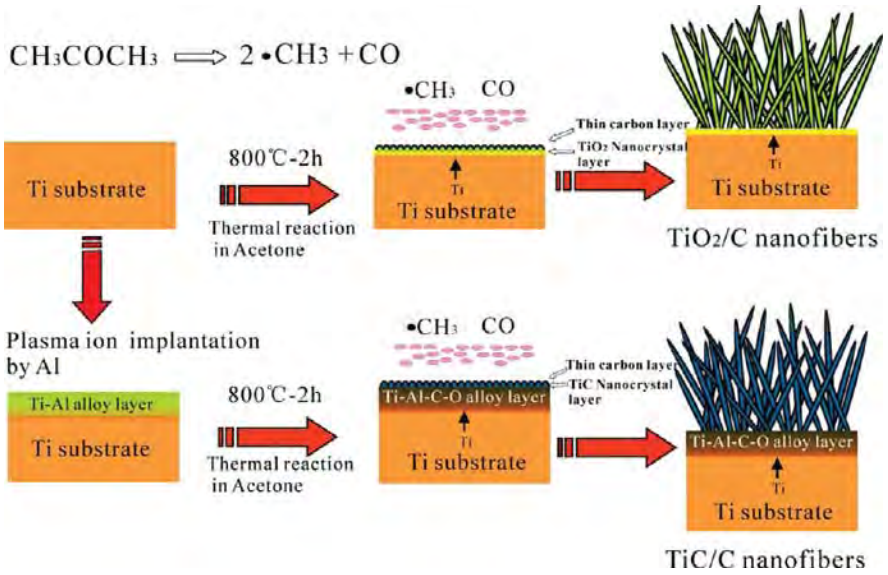

Figure 5. Schematic illustration of the in situ growth mechanism of the core–shell TiO_2/C and TiC/C NFs on Ti and Al ion-implanted Ti under flowing acetone at 800 °C.

The above results suggest that TiO_2/C NFs can be fabricated directly on Ti by a thermochemical reaction under flowing acetone at 800 °C without needing a template or foreign catalyst. Furthermore, after Al PIII, core–shell TiC/C NFs instead of TiO_2/C NFs can be produced. The overall reactions for the formation of core–shell TiO_2/C and TiC/C NFs on Ti or Al ion-implanted Ti foil at 800 °C are proposed as reactions 1 and 2

$$\begin{aligned} &Ti(s) + 2CH_3COCH_3(g) \\ &\quad = TiO_2(s) + 6C(s) + 6H_2(g)\ \Delta G \\ &\quad = -931.1\ kJ/mol \end{aligned} \tag{1}$$

$$\begin{aligned} &3Ti(s) + 2Al(s) + CH_3COCH_3(g) \\ &\quad = 3TiC(s) + Al_2O_3(s) + 6C(s) + 9H_2(g)\ \Delta G \\ &\quad = -2160.3\ kJ/mol \end{aligned} \tag{2}$$

$$\begin{aligned} &Ti(s) + CH_3COCH_3(g) \\ &\quad = TiC(s) + CO(g) + 6H_2(g)\ \Delta G \\ &\quad = -449.5\ kJ/mol \end{aligned} \tag{3}$$

According to thermodynamic analysis, Ti will react with acetone to form TiO_2 preferentially rather than TiC since the Gibbs free energy (ΔG) of reaction 1 to form TiO_2 is more negative than that of reaction 3 to form TiC. Thus, core–shell TiO_2/C is produced on pristine Ti substrate. However, in the presence of Al in the near surface of the Ti substrate after Al PIII, TiC is formed preferentially according to reaction 2 because of the more negative ΔG value.

The mechanism of this catalyst-free growth process to form core–shell TiO_2/C and TiC/C NFs is further described below and schematically illustrated in Figure 5. At 800 °C, acetone is decomposed into $\cdot CH_3$ radicals and CO,[24,27] and the CO generated in situ preferentially reacts with Ti to form TiO_2 by reaction 4 because of the more negative Gibbs free energy in compassion with reaction 5 to form TiC. At the same time, carbon atoms produced by decomposition of $\cdot CH_3$ radicals and reaction 4 precipitate on the surface of TiO_2 to form the carbon shell. As the reaction proceeds, more Ti atoms diffuse outward from the bulk through the boundary of the formed TiO_2 and react continuously with CO to form more TiO_2, finally core–shell TiO_2/C are obtained on the Ti foil as suggested by Figure 5.

$$\begin{aligned} &Ti(s) + 2CO(g) \\ &\quad = TiO_2(s) + 2C(graphite)\ \Delta G \\ &\quad = -361.9\ kJ/mol \end{aligned} \tag{4}$$

$$\begin{aligned} &Ti(s) + 2CO(g) \\ &\quad = TiC(s) + CO_2(g)\ \Delta G \\ &\quad = -158.9\ kJ/mol \end{aligned} \tag{5}$$

$$\begin{aligned} &Ti(s) + C(graphite) \\ &\quad = TiC(s)\ \Delta G \\ &\quad = -164.9\ kJ/mol \end{aligned} \tag{6}$$

$$\begin{aligned} &2Al(s) + 2CO(g) \\ &\quad = Al_2O_3(s) + 3C(graphite)\ \Delta G \\ &\quad = -811.9\ kJ/mol \end{aligned} \tag{7}$$

$$\begin{aligned} &4Al(s) + 3TiO_2(s) \\ &\quad = 2Al_2O_3(s) + 3Ti(s);\ \Delta G \\ &\quad = -538.2\ kJ/mol \end{aligned} \tag{8}$$

When Al is introduced into the surface of Ti by Al PIII, Ti preferentially reacts with C forming TiC rather than reacting with CO to produce TiO_2 because the ΔG for the reaction 7 between Al and CO to produce Al_2O_3 is more negative than that reaction 4 between Ti and CO to form TiO_2.[13,14,28,29] On

the other hand, the Al can reduce TiO_2 to Ti because of negative ΔG of reaction 8, and thus, reaction 6 can proceed preferentially in the presence of Al and thus core−shell TiC/C instead of TiO_2/C NFs are produced on the Al ion-implanted Ti as suggested by Figure 5. However, if the Al concentration is too high, a thick Al-enriched alloyed layer is formed as suggested by the GAXRD pattern in Figure 2e. This layer hinders Ti diffusion and restrains the NF growth extremely as suggested in Figure 2d. This technique constitutes an effective means to produce core−shell TiO_2/C and TiC/C NFs on Ti in a controllable fashion. Moreover, this one-step in situ synthetic technique is simple, economical, and easy to scale up.

These core/shell NFs grown directly on the Ti substrate may have good field-emission because of the good bonding and low resistance between the NFs and Ti substrate. Hence, their field-emission properties are investigated experimentally and compared to those of other reported 1D emitters. Figure 6a depicts the FE curves of the current density (J) versus applied field (E) for the TiC/C and TiO_2/C NFs on Ti foils. The turn-on field (E_{to}), which is usually defined as the electric field producing a current density of 10 μA/cm^2, is found to be 2.2 V/μm for TiC/C NFs and 3.2 V/μm for TiO_2/C NFs. The threshold fields E_{thr} (defined as the electric field for J = 1 mA/cm^2) for TiC/C NFs and TiO_2/C NFAs are 6.3 and 9.0 V/μm, respectively. Both the TiO_2/C and TiC/C NFs exhibit good field-emission stability throughout a period of 3 h experiment showing current density fluctuation of within 7 at % an average current of 1.2 mA/cm^2. Figure 6b shows the corresponding Fowler−Nordheim (F−N) plots for the two samples. The linearity exhibited by the F−N curve in the measurement range confirms that electron emission from the NFAs follows the F−N behavior. In comparison with the TiO_2/C NFAs, the TiC/C NFAs have lower E_{to} and E_{thr} and thus better field emission properties. As shown in Figure 2a,b, the TiC/C and TiO_2/C NFAs have similar morphology and structure and so they should have similar field emission factors. However, their FE performance is different and it can be attributed to the high electrical conductivity of the inner TiC, resulting in more effective electron transfer between the Ti substrate and C shell emitters. The electrical conductivity values of TiC, TiO_2, and C along the C-axis are 6.8 × 10^{-5}, 1600−10 000 and 0.17 Ω cm, respectively.[30−32] On the basis of these considerations, it is reasonable that the inner TiO_2 should not participate in the electron transport and emission from the TiO_2/C NFs due to the low conductivity of TiO_2. However, the highly conductive TiC inner core provides a more effective path for electron transfer between the cathode and outer C shell emitters due to the higher conductivity of TiC, thus yielding the enhanced field emission properties. The E_{to} and E_{thr} of the core−shell TiC/C NFAs fabricated directly on Ti is smaller than or comparable to those of C nanotube,[33] SiC nanowires,[34] ZnO nanowires,[35] TiO_2 nanowires,[36] as well as core−shell In/ZnS nanowires,[12] SiC/Al_2O_3 nanowires,[37] Zn/ZnO microcactuses,[38] AlN/BCN nanocones,[10] Si/C nanocones,[11] and SiC/C nanowires.[39] A detailed comparison is shown in Table 1, which indicates that the TiC/C NFs have better field-emission properties. The promising FE characteristics demonstrated by the TiC/C NFs are attractive to their potential applications to flat panel displays and vacuum nanoelectronic devices.

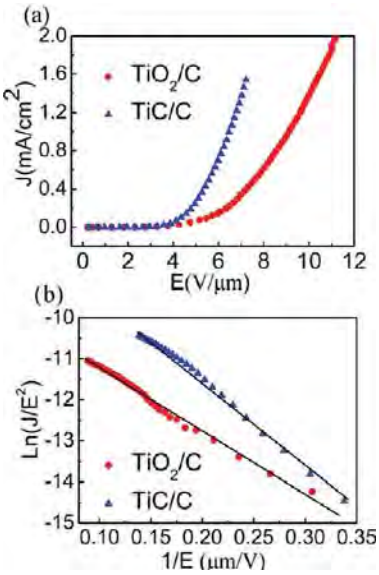

Figure 6. (a) FE current density (J) as a function of the applied electric field (E) and (b) corresponding F−N plot of the ln(J/E^2) versus 1/E for the core−shell TiO_2/C and TiC/C NFAs.

Table 1. Comparison of Typical Field-Emission Properties of Some Representative 1D Nanostructure Emitters

emitter	E_{to} (V/μm)	E_{thr} (V/μm)	ref
C nanotubes	2.12 at 10 μA/cm^2	3.03 at 0.5 mA/cm^2	33
SiC nanowires	5.0 at 10 μA/cm^2	8.5 at 10 mA/cm^2	34
ZnO nanowires	7.1 at 1 μA/cm^2	10.1 at 10 μA/cm^2	35
TiO_2 nanowires	4.2 at 10 μA/cm^2	11.5at 1 mA/cm^2	36
Si/C nanocones	2.52 at 1 μA/cm^2	8 at 0.1 mA/cm^2	11
SiC/C nanowires	4.2 at 10 μA/cm^2	5.1 at 0.1 mA/cm^2	39
AlN/BCN nanocones	7.8 at 10 μA/cm^2	14.8 at 10 μA/cm^2	10
In/ZnS nanowires	5.5 at 10 μA/cm^2	7.45 at 1.1 mA/cm^2	12
SiC/Al_2O_3 nanowires	10.4 at 1 mA/cm^2	13.8 at 10 mA/cm^2	37
Zn/ZnO microcaces	14.15 at 10 μA/cm^2	18.76 at 10 mA/cm^2	38
TiO_2/C nanofibers	3.2 at 10 μA/cm^2	9 at 1 mA/cm^2	Our work
TiC/C nanofibers	2.2 at 10 μA/cm^2	6.3 at 1 mA/cm^2	Our work

CONCLUSION

Core−shell TiO_2/C and TiC/C NFs are fabricated in situ on Ti or Al ion-implanted Ti samples thermochemically under flowing acetone at 800 °C. The Ti foil serves as both the Ti source and substrate for the core−shell TiO_2/C and TiC/C NFs to ensure strong bonding and small contact resistance between the Ti substrate and the core−shell field emitters. This configuration bodes well for FE as confirmed by this study. Introduction of Al by plasma immersion ion immersion enhances nucleation and growth of TiC because Al has a higher affinity to oxygen than Ti and the Gibbs free energy for the formation of Al_2O_3 is more negative than that of TiO_2. Hence, Ti reacts preferentially with C forming TiC rather than TiO_2 producing the TiC/C NFs on the Al ion-implanted Ti foil. However, if the Al concentration is too large, an Al-rich surface alloyed layer is formed to block Ti out-diffusion. The field emission performance of the core−shell TiC/C and TiO_2/C nanofiber arrays obeys the Fowler−Nordheim behavior with low turn-on fields of 2.2 and 3.2 V/μm, respectively. The enhanced field emission properties of TiC/C NFAs are

attributed to the synergetic effects of the highly conductive TiC inner core and outer C shell. The conductive TiC inner core provides an effective pathway for electron transfer between the cathode and outer C shell emitters. This technique offers a simple and economical means to synthesize core−shell TiO_2/C and TiC/C NFAs on Ti in one step and the resulting nanostructures are attractive to vacuum nanoelectronic devices.

AUTHOR INFORMATION

Corresponding Author

*E-mail: kaifuhuo@cityu.edu.hk or kfhuo@wust.edu.cn (K.H.); paul.chu@cityu.edu.hk (P.K.C.).

Notes

The authors declare no competing financial interest.

ACKNOWLEDGMENTS

This work was jointly supported by City University of Hong Kong Strategic Research Grant (SRG) #7008009, Hong Kong Research Grants Council (RGC) General Research Funds (GRF) #CityU 112510, and National Natural Science Foundation of China #50902104.

REFERENCES

(1) Xu, N. S.; Huq, S. E. *Mater. Sci. Eng., R* **2005**, *48* (2−5), 47−189.
(2) Milne, W. I.; Teo, K. B. K.; Amaratunga, G. A. J.; Legagneux, P.; Gangloff, L.; Schnell, J. P.; Semet, V.; Thien Binh, V.; Groening, O. *J. Mater. Chem.* **2004**, *14* (6), 933−943.
(3) Fang, X.; Bando, Y.; Gautam, U. K.; Ye, C.; Golberg, D. *J. Mater. Chem.* **2008**, *18* (5), 509−522.
(4) Patil, S. S.; Koinkar, P. M.; Dhole, S. D.; More, M. A.; Murakami, R.-i. *Phys. B: Condens. Matter* **2011**, *406* (9), 1809−1813.
(5) Kim, W. J.; Lee, J. S.; Lee, S. M.; Song, K. Y.; Chu, C. N.; Kim, Y. H. *ACS Nano* **2010**, *5*, 429−435.
(6) Lahiri, I.; Seelaboyina, R.; Hwang, J. Y.; Banerjee, R.; Choi, W. *Carbon* **2010**, *48* (5), 1531−1538.
(7) Talapatra, S.; Kar, S.; Pal, S. K.; Vajtai, R.; CiL.; Victor, P.; Shaijumon, M. M.; Kaur, S.; Nalamasu, O.; Ajayan, P. M. *Nat. Nanotechnol.* **2006**, *1* (2), 112−116.
(8) Matsuda, Y.; Deng, W.-Q.; Goddard, W. A. *J. Phys.Chem.C* **2007**, *111* (29), 11113−11116.
(9) Zhang, J.; Wang, X.; Yang, W.; Yu, W.; Feng, T.; Li, Q.; Liu, X.; Yang, C. *Carbon* **2006**, *44* (3), 418−422.
(10) Qian, W.; Zhang, Y.; Wu, Q.; He, C.; Zhao, Y.; Wang, X.; Hu, Z. *J. Phys. Chem. C* **2011**, *115* (23), 11461−11465.
(11) Wang, Q.; Li, J. J.; Ma, Y. J.; Bai, X. D.; Wang, Z. L.; Xu, P.; Shi, C. Y.; Quan, B. G.; Yue, S. L.; Gu, C. Z. *Nanotechnology* **2005**, *16*, 2919−2922.
(12) Gautam, U. K.; Fang, X.; Bando, Y.; Zhan, J.; Golberg, D. *ACS Nano* **2008**, *2* (5), 1015−1021.
(13) Li, A. J.; Hu, C. F.; Li, M. S.; Zhou, Y. C. *J. Eur. Ceram. Soc.* **2009**, *29* (12), 2619−2625.
(14) Hu, L. S.; Huo, K. F.; Chen, R. S.; Zhang, X. M.; Fu, J. J.; Chu, P. K. *Chem. Commun.* **2010**, *46* (36), 6828−6830.
(15) Wu, G. S.; Gong, L.; Feng, K.; Wu, S. L.; Zhao, Y.; Chu, P. K. *Mater. Lett.* **2011**, *65* (4), 661−663.
(16) Xin, Y. C.; Chu, P. K. Plasma Immersion Ion Implantation (PIII) of Light Alloys. In *Surface Engineering of Light Alloys*; Dong, H. S., Ed.; CRC Press and Woodhead Publishing: Abington, U.K., 2010; pp 362−397.
(17) Polyak, Y.; Bastl, Z. *Surf. Interface Anal.* **2009**, *41* (10), 830−833.
(18) Li, H.; Belkind, A.; Jansen, F.; Orban, Z. *Surf. Coat. Technol.* **1997**, *92* (3), 171−177.
(19) Qi, S. R.; Huang, X. T.; Gan, Z. W.; Ding, X. X.; Cheng, Y. *J. Cryst. Growth* **2000**, *219* (4), 485−488.
(20) Daothong, S.; Songmee, N.; Thongtem, S.; Singjai, P. *Scr. Mater.* **2007**, *57*, 567−570.
(21) Huo, K. F.; Hu, Y. M.; Ma, Y. W.; Lu, Y. N.; Hu, Z.; Chen, Y. *Nanotechnology* **2007**, *18*, 145615.
(22) Ma, H. L.; Yang, J. Y.; Dai, Y.; Zhang, Y. B.; Lu, B.; Ma, G. H. *Appl. Surf. Sci.* **2007**, *253* (18), 7497−7500.
(23) Lohse, B. H.; Calka, A.; Wexler, D. *J. Alloys Compd.* **2007**, *434*−*435*, 405−409.
(24) Montoro, L. A.; Corio, P.; Rosolen, J. M. *Carbon* **2007**, *45*, 1234−1241.
(25) Urbonaite, S.; Hälldahl, L.; Svensson, G. *Carbon* **2008**, *46* (14), 1942−1947.
(26) Chen, R.; Hu, L.; Huo, K.; Fu, J.; Ni, H.; Tang, Y.; Chu, P. K. *Chem.—Eur. J.* **2011**, *17* (51), 14552−14558.
(27) Sato, K.; Hidaka, Y. *Combust. Flame* **2000**, *122* (3), 291−311.
(28) Yeh, C. L.; Kuo, C. W.; Chu, Y. C. *J. Alloys Compd.* **2010**, *494*, 132−136.
(29) Legzdina, D.; Robertson, I. M.; Birnbaum, H. K. *Acta Mater.* **2005**, *53* (3), 601−608.
(30) Klimiec, E.; Stobierski, L.; Nowak, S.; Zaraska, W.; Kuczyński, S. *J. Electroceram.* **2011**, *26* (1), 90−98.
(31) Earle, M. D. *Phys. Rev.* **1942**, *61* (1−2), 56−62.
(32) Han, M.; Chan, S. H.; Jiang, S. P. *J. Power Sources* **2006**, *159* (2), 1005−1014.
(33) Rakhi, R. B.; Sethupathi, K.; Ramaprabhu, S. *Appl. Surf. Sci.* **2008**, *254* (21), 6770−6774.
(34) Wu, Z. S.; Deng, S. Z.; Xu, N. S.; Chen, J.; Zhou, J.; Chen, J. *Appl. Phys. Lett.* **2002**, *80*, 3829.
(35) Li, C.; Fang, G.; Yuan, L.; Liu, N.; Li, J.; Li, D.; Zhao, X. *Appl. Surf. Sci.* **2007**, *253* (20), 8478−8482.
(36) Huo, K. F.; Zhang, X. M.; Fu, J. J.; Qian, G. X.; Xin, Y. C.; Zhu, B. Q.; Ni, H. W.; Chu, P. K. *J. Nanosci. Nanotechnol.* **2009**, *9* (5), 3341−3346.
(37) Cui, H.; Gong, L.; Sun, Y.; Yang, G. Z.; Liang, C. L.; Chen, J.; Wang, C. X. *CrystEngComm* **2011**, *13* (5), 1416−1421.
(38) Khan, W. S.; Cao, C.; Chen, Z.; Nabi, G. *Mater. Chem. Phys.* **2010**, *124* (1), 493−498.
(39) Ryu, Y.; Park, B.; Song, Y.; Yong, K. *J. Cryst. Growth* **2004**, *271* (1−2), 99−104.